Generation of Current Vortex by Spin Current in Rashba Systems

Florian Lange,[1,*] Satoshi Ejima®,[1,2] Junji Fujimoto®,[3] Tomonori Shirakawa®,[4] Holger Fehske®,[1]
Seiji Yunoki,[2,4,5] and Sadamichi Maekawa®[5,3,†]

[1]*Institut für Physik, Universität Greifswald, 17489 Greifswald, Germany*
[2]*RIKEN Cluster for Pioneering Research (CPR), Wako, Saitama 351-0198, Japan*
[3]*Kavli Institute for Theoretical Sciences, University of Chinese Academy of Sciences, Beijing 100190, China*
[4]*RIKEN Center for Computational Science (R-CCS), Kobe, Hyogo 650-0047, Japan*
[5]*RIKEN Center for Emergent Matter Science (CEMS), Wako, Saitama 351-0198, Japan*

Employing unbiased large-scale time-dependent density-matrix renormalization-group simulations, we demonstrate the generation of a charge-current vortex via spin injection in the Rashba system. The spin current is polarized perpendicular to the system plane and injected from an attached antiferromagnetic spin chain. We discuss the conversion between spin and orbital angular momentum in the current vortex that occurs because of the conservation of the total angular momentum and the spin-orbit interaction. This is in contrast to the spin Hall effect, in which the angular-momentum conservation is violated. Finally, we predict the electromagnetic field that accompanies the vortex with regard to possible future experiments.

The interconversion of charge and spin degrees of freedom is a key issue in spintronics [1]. Noteworthy phenomena in this regard are the spin Hall effect, which describes the generation of a transverse spin current by a charge current, and its inverse [2–5]. These effects are due to a spin asymmetry of conduction electrons by the spin-orbit coupling. A typical model for studying the spin-charge interconversion is the two-dimensional electron gas with Rashba spin-orbit coupling [6,7]. Various effects due to the Rashba spin-orbit coupling have been extensively investigated, including the spin-orbit torque [8] and the Edelstein effect [9,10]. While the spin Hall conductivity actually vanishes in the Rashba model with quadratic dispersion [11–14], spin Hall physics may still be observed in mesoscopic Rashba systems. It was shown, for example, that a charge current in a nanowire can induce spin accumulation at the lateral edges [15].

In this Letter, we investigate a junction in which a spin current is transmitted into a Rashba system from an antiferromagnetic spin-1/2 Heisenberg chain. The spin current in the spin chain is carried by elementary excitations called spinons [16]. Our goal is to demonstrate the conversion of this spinon spin current into a conduction-electron spin current in the Rashba system and, in particular, to investigate the charge-current signal caused by the interplay of the spin injection and spin-orbit coupling. Although the junction is an interacting quantum system, it can nevertheless be efficiently simulated by using matrix-product-state methods [17–19] combined with a Lanczos transformation of the Rashba system [20–23], allowing us to obtain unbiased numerical results for the current dynamics. Most notably, we show that, when a spin current with

spin polarization perpendicular to the system is injected at a pointlike contact into the Rashba system, a charge-current vortex emerges. This is similar to the spin-charge conversion in the inverse spin Hall effect. What is different in our model, however, is that the direction of the current is not uniform and the system instead has a rotational symmetry around the injection point. The junction thus has a conserved total angular momentum, and it turns out that the injected spin angular momentum is mostly converted to orbital angular momentum of the current vortex. We focus on a model with an antiferromagnetic spin chain as a spin injector. As discussed in the Supplemental Material [24], the generation of the charge-current vortex could also be observed in other settings. At the end, we will discuss the relevance of our results for possible experiments.

Let us first introduce the setup in more detail. We consider a Rashba model in the xy plane on an infinite square lattice with sites $r \in \mathbb{Z}^2$,

$$\hat{H}_R = -\mu \sum_r \sum_{\sigma=\uparrow,\downarrow} \hat{c}^\dagger_{r,\sigma}\hat{c}_{r,\sigma} - t_R \sum_{\langle rr' \rangle} \sum_{\sigma=\uparrow,\downarrow} \hat{c}^\dagger_{r,\sigma}\hat{c}_{r',\sigma}$$
$$- i\lambda \sum_r (\hat{c}^\dagger_r \sigma^y \hat{c}_{r+e_x} - \hat{c}^\dagger_r \sigma^x \hat{c}_{r+e_y} - \text{H.c.}), \quad (1)$$

where μ is the chemical potential, t_R is the hopping, λ is the spin-orbit-coupling strength, σ^x and σ^y are Pauli matrices, and $\hat{c}_r = (\hat{c}_{r\uparrow}, \hat{c}_{r\downarrow})^T$ are fermion annihilation operators. One site r_0 shall be coupled to another system that is used to inject a spin current polarized in the z direction (see Fig. 1). Specifically, we employ an antiferromagnetic spin-1/2 Heisenberg chain of length N_S,
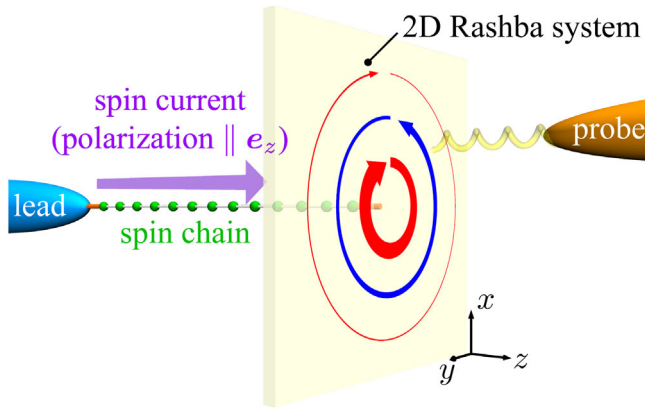
FIG. 1. Sketch of the setup described by Eqs. (1)–(4). A spin current (purple arrow) polarized perpendicular to the Rashba plane is induced in the spin chain by switching on a spin voltage in the lead. This spin current is injected into the Rashba system, where it causes the formation of a charge-current vortex (red and blue arrows). The orange segments denote the coupling between the spin chain and the lead and Rashba systems. In an experiment, the magnetic field induced by the charge current may be detected using scanning probe microscopy.

$$\hat{H}_S = J \sum_{j \geq 1}^{N_S - 1} \hat{\mathbf{S}}_j \hat{\mathbf{S}}_{j+1}, \qquad J > 0. \tag{2}$$

To generate a spin-current flow, the other end of the spin chain is connected to a one-dimensional semi-infinite tight-binding chain that serves as a spin reservoir,

$$\hat{H}_L(t) = -t_L \sum_{j \geq 1} \sum_{\sigma} (\hat{c}_{j,\sigma}^\dagger \hat{c}_{j+1,\sigma} + \text{H.c.})$$
$$- \Theta(t) \frac{V}{2} \sum_{j \geq 1} (\hat{c}_{j,\uparrow}^\dagger \hat{c}_{j,\uparrow} - \hat{c}_{j,\downarrow}^\dagger \hat{c}_{j,\downarrow}). \tag{3}$$

The second term in Eq. (3) describes a spin voltage that is switched on at time $t = 0$. Finally, the coupling between the subsystems is given by

$$\hat{H}_C = \frac{J'}{2} \sum_{\nu = x,y,z} \hat{S}_{N_S}^\nu (\hat{c}_{r_0}^\dagger \sigma^\nu \hat{c}_{r_0}) + \frac{J''}{2} \sum_{\nu = x,y,z} \hat{S}_1^\nu (\hat{c}_1^\dagger \sigma^\nu \hat{c}_1), \tag{4}$$

with J', $J'' > 0$, i.e., an antiferromagnetic Heisenberg interaction. The complete Hamiltonian then becomes $\hat{H}(t) = \hat{H}_R + \hat{H}_S + \hat{H}_L(t) + \hat{H}_C$. It is assumed that the composite system is initially in the ground state of $\hat{H}(t < 0)$ until the spin voltage is switched on. Throughout this Letter, we use t_R as the unit of energy and set $N_S = 12$, $J = t_L = 2$, $\mu = -3.5$, and $V = 0.5$. Since $\hat{H}(t)$ conserves the particle number in each tight-binding system, no charge current is injected in addition to the spin current. We are interested in the charge current that instead develops as a consequence of the injected spin current and the spin-orbit coupling. Here, the
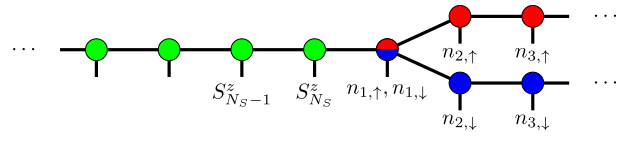

FIG. 2. Tensor-network-state ansatz for the numerical simulations. The vertical lines denote the physical indices, i.e., the basis states of the local Hilbert spaces. Here, they correspond to the occupation numbers $n_{j,\sigma}$ of the fermions in the Lanczos basis or, in the spin chain, the z components S_j^z of the spins. The remaining lines indicate the bond indices of the tensor network. On the left side, the one-dimensional lead is similarly split into two branches (not shown).

charge-current-density operators for neighboring sites $\mathbf{r}$ and $\mathbf{r} + \mathbf{e}_{x,y}$ are defined by $\hat{j}_{\mathbf{r},\mathbf{r}+\mathbf{e}_x}^c = \hat{c}_{\mathbf{r}}^\dagger(-it_R I + \lambda\sigma^y)\hat{c}_{\mathbf{r}+\mathbf{e}_x} +$ H.c. and $\hat{j}_{\mathbf{r},\mathbf{r}+\mathbf{e}_y}^c = \hat{c}_{\mathbf{r}}^\dagger(-it_R I - \lambda\sigma^x)\hat{c}_{\mathbf{r}+\mathbf{e}_y} +$ H.c., with I being the unit matrix in spin space, so that the total current at site $\mathbf{r}$ is

$$\hat{\mathbf{j}}_{\mathbf{r}}^c = \frac{1}{2}[(\hat{j}_{\mathbf{r},\mathbf{r}+\mathbf{e}_x}^c + \hat{j}_{\mathbf{r}-\mathbf{e}_x,\mathbf{r}}^c)\mathbf{e}_x + (\hat{j}_{\mathbf{r},\mathbf{r}+\mathbf{e}_y}^c + \hat{j}_{\mathbf{r}-\mathbf{e}_y,\mathbf{r}}^c)\mathbf{e}_y]. \tag{5}$$

In order to simulate the above model numerically, we use a Lanczos transformation that maps the two-dimensional Rashba system to a chain representation [20,23]. The Hamiltonian then becomes purely one-dimensional and matrix-product-state techniques can be used to calculate the ground state and simulate the time evolution with high accuracy [17–19]. To be precise, we utilize a tensor-network representation in which each tight-binding chain is split into two branches corresponding to different spin indices (pseudospin indices for the Rashba case) [23,26]. This significantly reduces the numerical effort compared with a regular matrix-product state. Figure 2 displays the tensor network in the usual graphical notation.

For the numerical calculations, the tight-binding chain and the Lanczos representation of the Rashba system are each truncated to 500 sites. The time evolution is carried out using the time-evolving block decimation with a second-order Suzuki-Trotter decomposition and a time step 0.025 [18]. For all simulated times, the truncation error is kept below 10^{-7}. In the Supplemental Material [24], the Lanczos transformation and the accuracy of the numerical results are discussed in further detail.

When the spin voltage is switched on in the first lead, a spin current starts to flow at the interface with the spin chain. The perturbation spreads through the chain, approximately with the spinon velocity $J\pi/2$, and finally reaches the Rashba system. At low temperatures, the efficiency of the spin injection into the Rashba system depends strongly on the coupling J' [27–29]. We have chosen $J'/J = 2.15$ and $J''/J = 1.70$ in order to maximize the spin current in the steady state. For these parameters, the spin current into

the Rashba system quickly saturates to a value slightly below $V/(4\pi)$, which is the current corresponding to the expected linear spin conductance of the junction with ideal contacts. In the following, we analyze the charge current induced by this continuous spin-current injection. We assume that the spin current is polarized in the z direction. Results for an x-polarized spin current are presented and briefly discussed in the Supplemental Material [24].

Figure 3 shows the numerically calculated charge-current profile for spin-orbit coupling parameters $\lambda = 0.1$ and 0.2 and different simulated times t. Clearly, multiple rings with circular charge current develop and then persist for long times. Neighboring rings have opposite orientation; i.e., the current alternates between clockwise and counterclockwise. This behavior can be understood qualitatively as
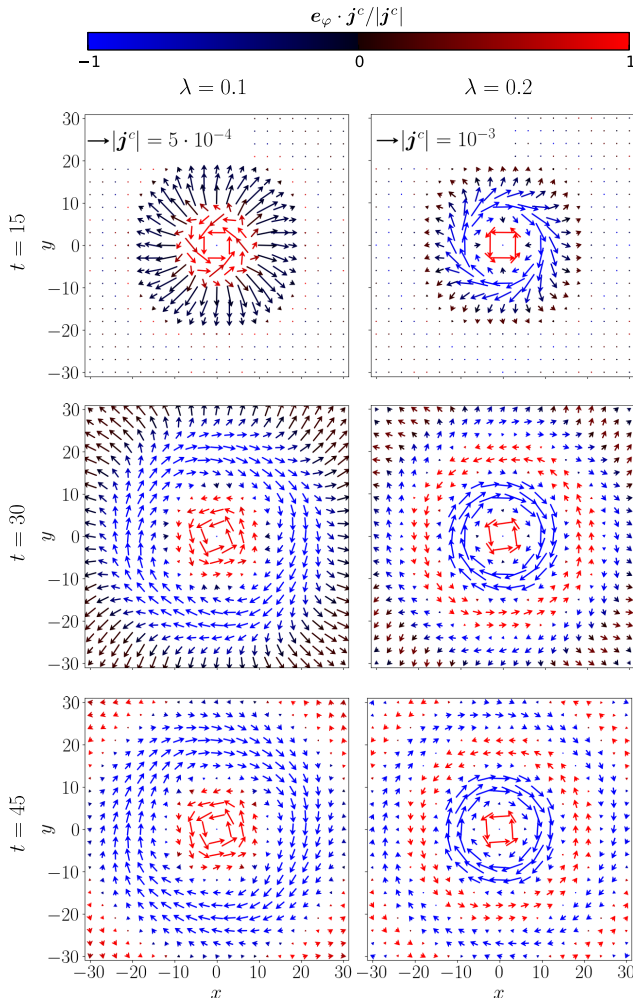
follows: A spin current in the Rashba system generates a transverse charge current via the inverse spin Hall effect [30]. Here, the spin current points in the radial direction relative to the injection point, which leads to the observed circular charge current. Because of the Rashba spin precession, the spin current oscillates as a function of the distance r from the injection point, so that the charge current eventually changes direction as r is increased. While the charge current at long times (and fixed radius r) is almost entirely azimuthal, the current in the transient regime clearly has a significant radial component. This current occurs because of the different velocities for particle and hole excitations at finite spin voltage V. Its magnitude depends approximately quadratically on V [24], since it is affected by both the strength of the injected spin current and the average velocity difference. For realistic values of V, the radial current should thus be very small. It should also be noted that, in a real system, the charge separation would be counteracted by the generated electrostatic potential, which is not accounted for in our model.

To make analytical predictions for the induced charge current that can be compared with the numerical results, it is more convenient to work with the continuous Rashba Hamiltonian

$$\hat{\mathcal{H}}_R = \hat{\boldsymbol{p}}^2/2m + \alpha(\sigma^x \hat{p}_y - \sigma^y \hat{p}_x). \tag{6}$$

By setting $m = 1/(2t_R)$ and $\alpha = -2\lambda$, $\hat{\mathcal{H}}_R$ can be used to analyze the lattice version Eq. (1) in the long-wavelength limit $k \to 0$. The continuum results are therefore applicable if the spin-orbit-coupling strength λ is small and the Fermi energy ε_F is close to the bottom of the electron bands (working at zero temperature, μ becomes the Fermi energy ε_F). In this regime, the wave number of the Rashba precession is $k_R = 2\lambda$, which agrees with the widths of the observed current rings.

Figure 4 shows the radial dependence of the current for the largest simulated time $t = 45$ in more detail. Here, the charge current is separated into two parts, $\hat{\boldsymbol{j}}_t^c$ and $\hat{\boldsymbol{j}}_\lambda^c$, which

FIG. 3. Snapshot of the charge-current densities $\boldsymbol{j}_r^c$ at different times t. For easier visualization, each arrow corresponds to the average value of the currents in a square of 3×3 sites. The length and color of the arrows indicate the magnitude and direction of the current, respectively. Black arrows show that the current points in the radial direction, while blue (red) arrows denote current in the clockwise (counterclockwise) azimuthal direction.
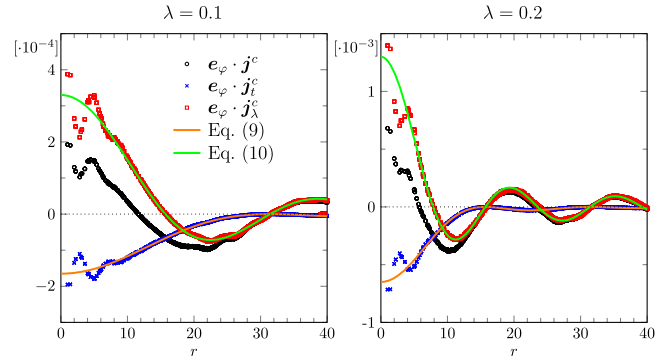

FIG. 4. Radial dependence of the azimuthal component of the charge current at time $t = 45$. The solid lines are according to Eqs. (9) and (10).

are the terms proportional to t_R and λ, respectively. Namely, we define

$$\hat{\boldsymbol{j}}^c_{t_R,\boldsymbol{r}} = \frac{it_R}{2}[\hat{c}^\dagger_{\boldsymbol{r}}(\hat{c}_{\boldsymbol{r}-\boldsymbol{e}_x} - \hat{c}_{\boldsymbol{r}+\boldsymbol{e}_x}) - \text{H.c.}]\boldsymbol{e}_x$$
$$+ \frac{it_R}{2}[\hat{c}^\dagger_{\boldsymbol{r}}(\hat{c}_{\boldsymbol{r}-\boldsymbol{e}_y} - \hat{c}_{\boldsymbol{r}+\boldsymbol{e}_y}) - \text{H.c.}]\boldsymbol{e}_y, \quad (7)$$

$$\hat{\boldsymbol{j}}^c_{\lambda,\boldsymbol{r}} = \frac{\lambda}{2}[\hat{c}^\dagger_{\boldsymbol{r}}\sigma^y(\hat{c}_{\boldsymbol{r}+\boldsymbol{e}_x} + \hat{c}_{\boldsymbol{r}-\boldsymbol{e}_x}) + \text{H.c.}]\boldsymbol{e}_x$$
$$- \frac{\lambda}{2}[\hat{c}^\dagger_{\boldsymbol{r}}\sigma^x(\hat{c}_{\boldsymbol{r}+\boldsymbol{e}_y} + \hat{c}_{\boldsymbol{r}-\boldsymbol{e}_y}) + \text{H.c.}]\boldsymbol{e}_y. \quad (8)$$

The functional form of the two contributions can be explained using a semiclassical analysis in terms of wave packets deflected by a spin-orbit force [31]. Let us consider the trajectory of an electron wave packet at the Fermi energy ε_F that has average momentum $\boldsymbol{p}$ and is initially centered at $\boldsymbol{r} = 0$ with the spin pointing up. In addition to propagating in the direction of $\boldsymbol{p}$, it experiences an effective transverse force proportional to the z component of the spin and the magnitude p of the momentum. Since the spin oscillates with wave number k_R because of the spin-orbit coupling, so does the deflecting force. This transverse movement corresponds to the spin-orbit part $\boldsymbol{j}^c_\lambda$ of the charge current. Furthermore, it causes the momentum $\boldsymbol{p}$ to no longer point in the radial direction $\boldsymbol{e}_r = (x,y)^T/r$, so that the regular part $\boldsymbol{j}^c_t$ of the current obtains a finite component in the azimuthal direction $\boldsymbol{e}_\varphi = (-y,x)^T/r$ as well. By assuming that the injected spin current is composed in equal parts of wave packets for spin-$\uparrow$ electrons and spin-$\downarrow$ holes that are evenly distributed over all directions, one obtains the following prediction for the charge current for long times t and small λ:

$$\boldsymbol{j}^c_t(r) = j^z\frac{2A}{k_R}\frac{\sin^2(k_R r/2)}{r^2}\boldsymbol{e}_\varphi, \quad (9)$$

$$\boldsymbol{j}^c_\lambda(r) = -j^z A\frac{\sin(k_R r)}{r}\boldsymbol{e}_\varphi, \quad (10)$$

where $A = 2\lambda/(v_F\pi)$ is a constant that depends on the Fermi velocity $v_F = 2t_R\sqrt{4 + (\lambda/t_R)^2 + \varepsilon_F/t_R}$, and j^z is the injected spin current. Inserting for j^z the time-averaged value from the numerical simulations, we obtain excellent agreement with the numerically calculated charge current for $r \gtrsim 8$ (see Fig. 4), without any adjustable parameters. Deviations for small r are likely due to the lattice discretization.

Since the continuous Rashba Hamiltonian $\hat{\mathcal{H}}_R$ is symmetric under a simultaneous rotation of space and spin, the z component of the total angular momentum $\hat{J}^z = \hat{M} + \hat{S}^z$, where $\hat{M} = \hat{x}\hat{p}_y - \hat{y}\hat{p}_x$ is the orbital angular momentum, is conserved. While the lattice Hamiltonian $\hat{H}_R$ does not have this symmetry, we may expect the conservation of the total

angular momentum to hold approximately, when the Fermi energy is small and the lattice model behaves similar to the continuum model. To be concrete, we define the orbital angular momentum on the lattice as $\hat{M} = \hat{x}\sin(\hat{p}_y) - \hat{y}\sin(\hat{p}_x)$. Using the first-quantized version of Eq. (1), $\hat{H}_R = -2t_R[\cos(\hat{p}_x) + \cos(\hat{p}_y)]I - 2\lambda[\sigma^x\sin(\hat{p}_y) - \sigma^y\sin(\hat{p}_x)]$, one then obtains from the Heisenberg equation $d\hat{S}^z/dt = -2\lambda[\sin(\hat{p}_y)\sigma^y + \sin(\hat{p}_x)\sigma^x]$ and $d\hat{M}/dt = 2\lambda[\cos(\hat{p}_x)\sin(\hat{p}_y)\sigma^y + \cos(\hat{p}_y)\sin(\hat{p}_x)\sigma^x]$. Obviously, $\hat{S}^z + \hat{M}$ is approximately conserved if we confine our analysis to states with small momenta p. To calculate M in the interacting model numerically, we use the second-quantized expression

$$\hat{M} = -\frac{1}{2}\sum_{\boldsymbol{r}}\sum_{\sigma=\uparrow,\downarrow}[ix\hat{c}^\dagger_{\boldsymbol{r},\sigma}\hat{c}_{\boldsymbol{r}+\boldsymbol{e}_y,\sigma} - iy\hat{c}^\dagger_{\boldsymbol{r},\sigma}\hat{c}_{\boldsymbol{r}+\boldsymbol{e}_x,\sigma} + \text{H.c.}]. \quad (11)$$

Comparing with Eq. (7), one can see that $\hat{M}$ is determined by the regular part $\hat{\boldsymbol{j}}^c_t$ of the charge-current-density operator $\hat{\boldsymbol{j}}^c$.

When the spin current is injected, it increases the total angular momentum $J^z_R = S^z_R + M$ in the Rashba system. One might then ask how J^z_R is composed of the spin S^z_R and the orbital contribution M. Figure 5 displays the numerical results for the time evolution of the angular-momentum expectation values. As noted above, the total angular momentum is not exactly conserved but the deviation is relatively small for $\varepsilon_F = -3.5$. Initially, $M = S^z_R = 0$ because the spin current has not entered the Rashba system yet. The delay before the angular momenta visibly change is in agreement with the expectation $N_S/v_S \approx 3.8$ based on the spinon velocity $v_S = J\pi/2$ in the infinite chain. For short times after the spin
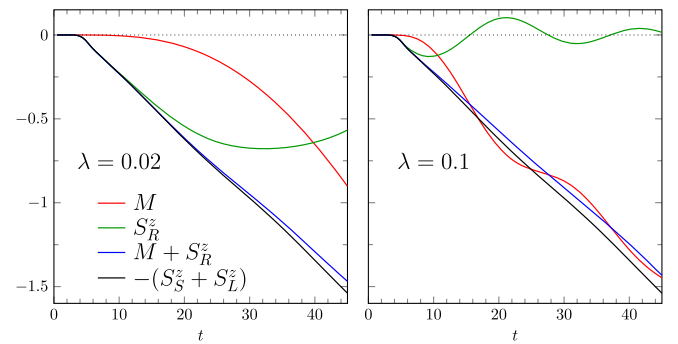

FIG. 5. Time evolution of the z component of the spin and orbital angular momentum in the Rashba system. The total spins in the lead and the spin chain are denoted by S^z_L and S^z_S, respectively. Therefore, the black line indicates the injected spin angular momentum. It would match the blue line if the total angular momentum was conserved.

current has reached the Rashba system, S_R^z makes up most of the angular momentum, while M remains approximately zero. On longer timescales, however, S_R^z can be seen to oscillate around zero, which means that eventually most of the injected spin angular momentum is converted to orbital angular momentum M. With the same assumptions used to derive Eqs. (9) and (10), one obtains that both the amplitude and the period of the oscillations are proportional to the wave number k_R of the Rashba precession. The numerical results roughly agree with these predictions, except that the oscillations in S_R^z and M also appear to decrease with time.

We estimate the magnetic field generated by the current vortex following the Biot-Savart law of electromagnetism. By assuming λ, a lattice constant of 1 Å, a hopping parameter $t_R = 1$ eV, and a linear dependence of the induced charge current on the spin voltage V, we obtain a field strength $B \approx V \times 10^{-5}$ T/eV at the center. For a realistic value of the spin voltage in the order of 10^{-4} eV, this is about 10^{-9} T and should therefore be within reach of experimental detection by scanning probe microscopy methods. To reach the necessary sensitivity, one could, e.g., use a nitrogen vacancy defect center in diamond as detector [32]. We moreover expect that the magnetic field would be larger in a perhaps more realistic setup with a bundle of spin chains instead of a single chain. Finally, one could also consider injecting an ac spin current into the two-dimensional electron gas, in which case the current vortex would emit an electromagnetic field of similar strength.

In conclusion, a charge-current vortex can be generated in a Rashba system by locally injecting a spin current. The formation of the current vortex is accompanied by the conversion of the injected spin angular momentum to orbital angular momentum. We demonstrated these effects for a generic model in which the spin current is transferred from an antiferromagnetic Heisenberg spin chain to a square-lattice Rashba system. In light of the recent realization of spin transport in the spin-chain material Sr_2CuO_3 [33], this model could be relevant from an experimental point of view. Accurate time-dependent density-matrix renormalization-group results for the charge current were found to agree well with predictions from semiclassical considerations. The charge-current vortex induces an electromagnetic field, which may be observed experimentally.

---

[*]langef@uni-greifswald.de
[†]sadamichi.maekawa@riken.jp
[1] S. Maekawa, S. Valenzuela, E. Saitoh, and T. Kimura, *Spin Current*, Oxford Science Publications (Oxford University Press, Oxford, 2015).
[2] J. E. Hirsch, Phys. Rev. Lett. **83**, 1834 (1999).
[3] S. Murakami, N. Nagaosa, and S.-C. Zhang, Science **301**, 1348 (2003).
[4] J. Sinova, D. Culcer, Q. Niu, N. A. Sinitsyn, T. Jungwirth, and A. H. MacDonald, Phys. Rev. Lett. **92**, 126603 (2004).
[5] J. Sinova, S. O. Valenzuela, J. Wunderlich, C. H. Back, and T. Jungwirth, Rev. Mod. Phys. **87**, 1213 (2015).
[6] Y. A. Bychkov and E. I. Rashba, JETP Lett. **39**, 78 (1984), http://www.jetpletters.ac.ru/ps/1264/article_19121.shtml.
[7] A. Manchon, H. C. Koo, J. Nitta, S. M. Frolov, and R. A. Duine, Nat. Mater. **14**, 871 (2015).
[8] A. Manchon, J. Železný, I. M. Miron, T. Jungwirth, J. Sinova, A. Thiaville, K. Garello, and P. Gambardella, Rev. Mod. Phys. **91**, 035004 (2019).
[9] V. Edelstein, Solid State Commun. **73**, 233 (1990).
[10] K. Shen, G. Vignale, and R. Raimondi, Phys. Rev. Lett. **112**, 096601 (2014).
[11] J.-i. Inoue, G. E. W. Bauer, and L. W. Molenkamp, Phys. Rev. B **70**, 041303(R) (2004).
[12] O. Chalaev and D. Loss, Phys. Rev. B **71**, 245318 (2005).
[13] E. I. Rashba, Phys. Rev. B **70**, 201309(R) (2004).
[14] P. L. Krotkov and S. Das Sarma, Phys. Rev. B **73**, 195307 (2006).
[15] B. K. Nikolić, S. Souma, L. P. Zârbo, and J. Sinova, Phys. Rev. Lett. **95**, 046601 (2005).
[16] *Quantum Magnetism*, edited by U. Schollwöck, J. Richter, D. J. J. Farnell, and R. F. Bishop (Springer, Berlin, Heidelberg, 2004).
[17] S. R. White, Phys. Rev. Lett. **69**, 2863 (1992).
[18] G. Vidal, Phys. Rev. Lett. **91**, 147902 (2003).
[19] A. Branschädel, G. Schneider, and P. Schmitteckert, Ann. Phys. (Berlin) **522**, 657 (2010).
[20] T. Shirakawa and S. Yunoki, Phys. Rev. B **90**, 195109 (2014).
[21] A. Allerdt, C. A. Büsser, G. B. Martins, and A. E. Feiguin, Phys. Rev. B **91**, 085101 (2015).
[22] A. Allerdt and A. E. Feiguin, Front. Phys. **7**, 67 (2019).
[23] F. Lange, S. Ejima, T. Shirakawa, S. Yunoki, and H. Fehske, J. Phys. Soc. Jpn. **89**, 044601 (2020).
[24] See Supplemental Material at http://link.aps.org/supplemental/10.1103/PhysRevLett.126.157202 for, which includes Ref. [25], for details on the numerical calculations, results for spin-current polarization parallel to the Rashba plane, a derivation of Eqs. (9) and (10), an alternative model

for spin injection, and a discussion of the radial charge current.

[25] V. Murg, F. Verstraete, O. Legeza, and R. M. Noack, Phys. Rev. B **82**, 205105 (2010).

[26] A. Holzner, A. Weichselbaum, and J. von Delft, Phys. Rev. B **81**, 125126 (2010).

[27] D. Morath, N. Sedlmayr, J. Sirker, and S. Eggert, Phys. Rev. B **94**, 115162 (2016).

[28] F. Lange, S. Ejima, T. Shirakawa, S. Yunoki, and H. Fehske, Phys. Rev. B **97**, 245124 (2018).

[29] F. Lange, S. Ejima, and H. Fehske, Europhys. Lett. **125**, 17001 (2019).

[30] E. M. Hankiewicz, L. W. Molenkamp, T. Jungwirth, and J. Sinova, Phys. Rev. B **70**, 241301(R) (2004).

[31] B. K. Nikolić, L. P. Zârbo, and S. Welack, Phys. Rev. B **72**, 075335 (2005).

[32] G. de Lange, D. Ristè, V. V. Dobrovitski, and R. Hanson, Phys. Rev. Lett. **106**, 080802 (2011).

[33] D. Hirobe, M. Sato, T. Kawamata, Y. Shiomi, K. Uchida, R. Iguchi, Y. Koike, S. Maekawa, and E. Saitoh, Nat. Phys. **13**, 30 (2017).

[34] M. Fishman, S. R. White, and E. M. Stoudenmire, arXiv: 2007.14822.